

Nonlinear hypocentre determination

Petr Bulant & Luděk Klimeš

*Department of Geophysics, Faculty of Mathematics and Physics, Charles University in Prague, Ke Karlovu 3, 121 16 Praha 2, Czech Republic,
<http://sw3d.cz/staff/bulant.htm>, <http://sw3d.cz/staff/klimes.htm>*

Summary

We consider the robust nonlinear approach to hypocentre determination proposed by Tarantola & Valette, consisting in direct evaluation of the nonnormalized 3-D marginal a posteriori density function which describes the relative probability of the seismic hypocentre. The nonnormalized 3-D marginal a posteriori density function is discretized at the gridpoints of a sufficiently dense 3-D spatial grid of points. This approach takes into account the inaccuracy of the velocity model and the corresponding influence on the hypocentre determination, estimates the uncertainty of the hypocentre position, and allows for testing the model covariance function describing the uncertainty of the velocity model. The model covariance function is projected onto the uncertainty of the hypocentral position through the geometrical covariances of theoretical travel times calculated in the velocity model.

For the sake of simplicity and rapid numerical implementation, we consider just the diagonal elements of the geometrical travel-time covariance matrix in this paper. We discuss the distortion of the nonnormalized 3-D marginal a posteriori density function caused by this simplification, and present a numerical example.

Keywords

Hypocentre determination, velocity model, accuracy of the velocity model, model covariance function, geometrical travel-time covariance matrix, marginal a posteriori density function of hypocentral coordinates, arrival-time residuals, arrival-time misfit.

1. Introduction

Determination of the position of the seismic hypocentre from measured arrival times of P and S waves is a frequently appearing task in seismology. To determine the probable position of the seismic hypocentre, we need a velocity model in addition to the measured arrival times. Unfortunately, this information is insufficient for determining the uncertainty of the hypocentral position, which may sometimes extent to infinity.

In order to estimate the uncertainty of the hypocentral position, we also need to know the uncertainty of the measured arrival times and the uncertainty of the velocity model. The uncertainty of the measured arrival times is expressed in terms of the data covariance matrix of the measured arrival times, which is usually diagonal and composed of the squares of the standard deviations of the measured arrival times. The uncertainty of the velocity model is expressed in terms of the model covariance function (Franklin, 1970; Tarantola & Valette, 1982; Tarantola & Nercessian, 1984; Tarantola, 1987; Klimeš, 2002a) which is projected onto the uncertainty of the hypocentral position through the geometrical covariances of theoretical travel times calculated in the velocity

model (Klimeš, 2002c, 2008). In order to estimate the uncertainty of the hypocentral position, we thus need the standard deviations of the measured arrival times, and the geometrical covariances of theoretical travel times calculated using the model covariance function.

In this paper, we follow Tarantola & Valette (1982) and concentrate on directly calculating the nonnormalized 3-D marginal a posteriori density function which describes the relative probability of the seismic hypocentre, discretized at the gridpoints of a sufficiently dense 3-D spatial grid of points. This nonlinear approach to the hypocentre determination is very promising, because the theoretical travel times from the receivers to the gridpoints of a 3-D spatial grid of points can efficiently be calculated in the velocity model using the controlled initial-value ray tracing (Bulant, 1999) followed by the interpolation of travel times within ray cells (Bulant & Klimeš, 1999). The algorithm of nonlinear hypocentre determination is proposed in Section 2. The result of the algorithm is the nonnormalized 3-D marginal a posteriori density function which describes the relative probability of the seismic hypocentre.

The maximum value of the nonnormalized 3-D marginal a posteriori density function resulting from the hypocentre determination algorithm yields the information on the “norm” of the minimum arrival-time residuals referred to as the “arrival-time misfit” in this paper, see Section 3.

The minimum arrival-time residuals carry information pertinent to the accuracy of the velocity model (Klimeš, 1996). This information can be used to check the consistency of the velocity model and measured arrival times with the given model covariance function and the given standard deviations of the measured arrival times. The mean value of the arrival-time misfit is estimated in Section 4. The mean value of the arrival-time misfits from various hypocentre determinations can then be compared with the mean value of the estimation derived in Section 4. This comparison is described in Section 5.

Unfortunately, we have not been able to sufficiently rapidly implement the numerical calculation of the whole geometrical travel-time covariance matrix at the gridpoints of a 3-D spatial grid, but we still wish to perform numerical tests of the proposed algorithm. We thus consider only the diagonal elements of the geometrical travel-time covariance matrix. This simplification leads to a considerable distortion of the nonnormalized 3-D marginal a posteriori density function describing the relative probability of the seismic hypocentre. Section 6 is devoted to this simplification and to the estimation of the distortion.

In Section 7, we then present the numerical example obtained using the incomplete geometrical travel-time covariance matrix.

2. Nonlinear hypocentre determination in a spatial grid of points

The parameter space of the kinematic hypocentre determination consists of three hypocentral coordinates x_i and hypocentral time x_4 . The data space consists of N measured arrival times corresponding to P waves or S waves. We denote the vector of N measured arrival times by \mathbf{d} .

The probability of measured arrival times is proportional to the nonnormalized data density function $\varrho_{\text{D}}(\mathbf{d})$. We assume that the data density function is Gaussian,

$$\varrho_{\text{D}}(\mathbf{d}) = \exp\left[-\frac{1}{2}(\mathbf{d}-\mathbf{t})^{\text{T}}\mathbf{T}^{-1}(\mathbf{d}-\mathbf{t})\right] \quad , \quad (1)$$

where \mathbf{t} is the vector of N mean measured arrival times and \mathbf{T} is the $N \times N$ data covariance matrix corresponding to the measured arrival times.

The relation between the data and parameters is described by the nonnormalized theoretical density function $\vartheta(\mathbf{d}, x_i, x_4)$. The theoretical density function describes the relation between the measured arrival times and the inaccurate theoretical travel times calculated in the inaccurate velocity model.

We assume that each arrival time corresponds to just one theoretical travel time from a possible hypocentral point x_i . In case of multiple theoretical travel times, we may consider each travel time separately and combine the resulting marginal a posteriori density functions. In case of no theoretical travel time from a possible hypocentral point x_i , the resulting marginal a posteriori density function is zero at x_i . We assume that the theoretical density function is Gaussian,

$$\vartheta(\mathbf{d}, x_i, x_4) = \exp\left[-\frac{1}{2}(\mathbf{d}-\tilde{\boldsymbol{\tau}})^{\text{T}}\boldsymbol{\Theta}^{-1}(\mathbf{d}-\tilde{\boldsymbol{\tau}})\right] \quad , \quad (2)$$

where $\boldsymbol{\Theta}$ is the $N \times N$ matrix of geometrical covariances of theoretical travel times, and

$$\tilde{\boldsymbol{\tau}}(x_i, x_4) = \boldsymbol{\tau}(x_i) + \mathbf{E} x_4 \quad . \quad (3)$$

Here $\boldsymbol{\tau}(x_i)$ is the vector of N theoretical travel times from the receivers to point x_i , x_4 is a possible hypocentral time, and \mathbf{E} is the vector composed of N unities.

A posteriori density function is (Tarantola & Valette, 1982, eq. 6-1)

$$\sigma(\mathbf{d}, x_i, x_4) = \varrho_{\text{D}}(\mathbf{d}) \varrho_{\text{P}}(x_i, x_4) \vartheta(\mathbf{d}, x_i, x_4) / \mu(\mathbf{d}, x_i, x_4) \quad . \quad (4)$$

In Cartesian coordinates, null information density function $\mu(\mathbf{d}, x_i, x_4)$ is unit,

$$\mu(\mathbf{d}, x_i, x_4) = 1 \quad , \quad (5)$$

and parameter a priori density function $\varrho_{\text{P}}(x_i, x_4)$ is unit,

$$\varrho_{\text{P}}(x_i, x_4) = 1 \quad . \quad (6)$$

The resulting marginal a posteriori density function of hypocentral coordinates and hypocentral time is (Tarantola & Valette, 1982, eq. 6-4)

$$\tilde{\sigma}_{\text{P}}(x_i, x_4) = \int \text{d}^N \mathbf{d} \sigma(\mathbf{d}, x_i, x_4) \quad . \quad (7)$$

We insert relation (4) with (1), (2), (5) and (6) into definition (7) and obtain

$$\tilde{\sigma}_{\text{P}}(x_i, x_4) = \int \text{d}^N \mathbf{d} \exp\left\{-\frac{1}{2}[(\mathbf{d}-\mathbf{t})^{\text{T}}\mathbf{T}^{-1}(\mathbf{d}-\mathbf{t}) + (\mathbf{d}-\tilde{\boldsymbol{\tau}})^{\text{T}}\boldsymbol{\Theta}^{-1}(\mathbf{d}-\tilde{\boldsymbol{\tau}})]\right\} \quad . \quad (8)$$

For integration, we assemble the terms with \mathbf{d} in the exponent in relation (8),

$$\tilde{\sigma}_{\mathbf{P}}(x_i, x_4) = \int d^N \mathbf{d} \exp\left\{-\frac{1}{2}[(\mathbf{d} - \mathbf{\Theta} \mathbf{S}^{-1} \mathbf{t} - \mathbf{T} \mathbf{S}^{-1} \tilde{\boldsymbol{\tau}})^{\mathbf{T}} (\mathbf{T}^{-1} + \mathbf{\Theta}^{-1})(\mathbf{d} - \mathbf{\Theta} \mathbf{S}^{-1} \mathbf{t} - \mathbf{T} \mathbf{S}^{-1} \tilde{\boldsymbol{\tau}}) + (\mathbf{t} - \tilde{\boldsymbol{\tau}})^{\mathbf{T}} \mathbf{S}^{-1} (\mathbf{t} - \tilde{\boldsymbol{\tau}})]\right\} \quad , \quad (9)$$

where

$$\mathbf{S} = \mathbf{T} + \mathbf{\Theta} \quad (10)$$

is the complete arrival-time covariance matrix, compare to Klimeš (2002a, eq. 34). After integration, we obtain

$$\tilde{\sigma}_{\mathbf{P}}(x_i, x_4) = \sigma_{\mathbf{P}}(x_i, x_4) \frac{(2\pi)^{\frac{N}{2}}}{\sqrt{\det(\mathbf{T}^{-1} + \mathbf{\Theta}^{-1})}} \quad , \quad (11)$$

where

$$\sigma_{\mathbf{P}}(x_i, x_4) = \exp\left[-\frac{1}{2}(\mathbf{t} - \tilde{\boldsymbol{\tau}})^{\mathbf{T}} \mathbf{S}^{-1} (\mathbf{t} - \tilde{\boldsymbol{\tau}})\right] \quad (12)$$

is the nonnormalized marginal a posteriori density function of hypocentral coordinates and hypocentral time.

We insert definition (3) and obtain

$$\sigma_{\mathbf{P}}(x_i, x_4) = \sigma_{\mathbf{P}3}(x_i) \exp\left[-\frac{1}{2}S^{-1}(x_4 - h)^2\right] \quad , \quad (13)$$

where

$$h = S \mathbf{E}^{\mathbf{T}} \mathbf{S}^{-1} (\mathbf{t} - \boldsymbol{\tau}) \quad (14)$$

is the mean value $\langle x_4 \rangle$ of hypocentral time $x_4(x_i)$ at point x_i . Here quantity S defined as

$$S^{-1} = \mathbf{E}^{\mathbf{T}} \mathbf{S}^{-1} \mathbf{E} \quad (15)$$

determines the standard deviation

$$\sqrt{\langle (x_4 - h)^2 \rangle} = \sqrt{S} \quad (16)$$

of hypocentral time $x_4(x_i)$ at point x_i . The nonnormalized 3-D marginal a posteriori density function in relation (13) reads

$$\sigma_{\mathbf{P}3}(x_i) = \exp\left\{-\frac{1}{2}[(\mathbf{t} - \boldsymbol{\tau})^{\mathbf{T}} \mathbf{S}^{-1} (\mathbf{t} - \boldsymbol{\tau}) - S^{-1} h^2]\right\} \quad . \quad (17)$$

The nonnormalized 3-D marginal a posteriori density function represents the maximum of nonnormalized marginal density function $\sigma_{\mathbf{P}}(x_i, x_4)$ over hypocentral time x_4 at point x_i .

Inserting (14) and (15) into (17), we can express the nonnormalized 3-D marginal a posteriori density function (17) of hypocentral coordinates as

$$\sigma_{\mathbf{P}3}(x_i) = \exp\left[-\frac{1}{2}(\mathbf{t} - \boldsymbol{\tau})^{\mathbf{T}} \mathbf{C}^{-1} (\mathbf{t} - \boldsymbol{\tau})\right] \quad , \quad (18)$$

where

$$\mathbf{C}^{-1} = \mathbf{S}^{-1} - \mathbf{S}^{-1} \mathbf{E} (\mathbf{E}^{\mathbf{T}} \mathbf{S}^{-1} \mathbf{E})^{-1} \mathbf{E}^{\mathbf{T}} \mathbf{S}^{-1} \quad (19)$$

is an $N \times N$ matrix of rank $N - 1$ with null space generated by vector \mathbf{E} .

3. Maximum of the nonnormalized marginal a posteriori density function of hypocentral coordinates

To obtain the maximum of the nonnormalized marginal a posteriori density function $\sigma_{P_3}(x_i)$ of hypocentral coordinates, we differentiate $\sigma_{P_3}(x_i)$ with respect to hypocentral coordinates x_i . We neglect the derivatives of matrix \mathbf{C}^{-1} , and obtain equation

$$\mathbf{P}^T \mathbf{C}^{-1} [\mathbf{t} - \boldsymbol{\tau}(x_i)] = 0 \quad (20)$$

for the coordinates x_i of the maximum. Here \mathbf{P} is the $N \times 3$ matrix of slowness vectors leading from the receivers, with elements

$$P_{Ji} = \frac{\partial \tau_J}{\partial x_i} \quad . \quad (21)$$

We expect that the maximum is located near the unknown exact hypocentre. We thus apply the linear expansion

$$\boldsymbol{\tau} = \boldsymbol{\tau}^0 + \mathbf{P}(\mathbf{x} - \mathbf{x}^0) \quad (22)$$

of travel times in the vicinity of unknown exact hypocentre x_i^0 . Vector \mathbf{x} represents the coordinates x_i of the maximum, vector \mathbf{x}^0 represents the coordinates x_i^0 of the exact hypocentre, and $\boldsymbol{\tau}^0$ is the vector of inaccurate theoretical travel times from the receivers to the exact hypocentre.

We insert linear expansion (22) into equation (20),

$$\mathbf{P}^T \mathbf{C}^{-1} [\mathbf{t} - \boldsymbol{\tau}^0 - \mathbf{P}(\mathbf{x} - \mathbf{x}^0)] = 0 \quad , \quad (23)$$

and calculate the mislocation of the maximum with respect to the unknown exact hypocentre,

$$\mathbf{x} - \mathbf{x}^0 = (\mathbf{P}^T \mathbf{C}^{-1} \mathbf{P})^{-1} \mathbf{P}^T \mathbf{C}^{-1} (\mathbf{t} - \boldsymbol{\tau}^0) \quad . \quad (24)$$

The arrival-time residuals at the maximum follow from linear expansion (22) with (24), and read

$$\mathbf{t} - \boldsymbol{\tau} = [\mathbf{1} - \mathbf{P}(\mathbf{P}^T \mathbf{C}^{-1} \mathbf{P})^{-1} \mathbf{P}^T \mathbf{C}^{-1}] (\mathbf{t} - \boldsymbol{\tau}^0) \quad . \quad (25)$$

Since $N \times N$ projection matrix $\mathbf{1} - \mathbf{P}(\mathbf{P}^T \mathbf{C}^{-1} \mathbf{P})^{-1} \mathbf{P}^T \mathbf{C}^{-1}$ has rank $N-3$ with null space generated by the three columns of matrix \mathbf{P} , the minimum arrival-time residuals do not depend on the exact position of the hypocentre (Klimeš, 1996).

The maximum value of the nonnormalized marginal a posteriori density function $\sigma_P(x_i, x_4)$ of hypocentral coordinates and hypocentral time is equal to the maximum value of the nonnormalized marginal a posteriori density function $\sigma_{P_3}(x_i)$ of hypocentral coordinates, and reads, see (18),

$$\sigma_{P_3}^{\max} = \exp \left(-\frac{1}{2} y \right) \quad , \quad (26)$$

where quantity

$$y = (\mathbf{t} - \boldsymbol{\tau})^T \mathbf{C}^{-1} (\mathbf{t} - \boldsymbol{\tau}) \quad , \quad (27)$$

with $\mathbf{t} - \boldsymbol{\tau}$ given by (25), represents the square of the “norm” of the minimum arrival-time residuals $\mathbf{t} - \boldsymbol{\tau}$. We shall refer to y as the “arrival-time misfit”.

The arrival-time residuals (25) are primarily the consequence of the inaccurate velocity model (Klimeš, 1996). The arrival-time misfit then contains information on the extent of the inaccuracy of the velocity model.

We insert (25) into (27) and obtain expression

$$y = (\mathbf{t} - \boldsymbol{\tau}^0)^T [\mathbf{C}^{-1} - \mathbf{C}^{-1} \mathbf{P}(\mathbf{P}^T \mathbf{C}^{-1} \mathbf{P})^{-1} \mathbf{P}^T \mathbf{C}^{-1}] (\mathbf{t} - \boldsymbol{\tau}^0) \quad . \quad (28)$$

for the arrival–time misfit.

The value of the arrival–time misfit can be obtained from the maximum $\sigma_{\mathbf{P}_3}^{\max}$ of the nonnormalized marginal a posteriori density function $\sigma_{\mathbf{P}_3}(x_i)$ of hypocentral coordinates as

$$y = -2 \ln(\sigma_{\mathbf{P}_3}^{\max}) \quad , \quad (29)$$

see (26).

We are now interested in the mean value of the stochastic distribution of arrival–time misfit y .

4. Mean value of the stochastic distribution of the arrival–time misfit

Arrival–time residuals $\mathbf{t} - \tilde{\boldsymbol{\tau}}^0$ corresponding to exact hypocentral coordinates x_i^0 and exact hypocentral time x_4^0 are caused by inaccurate picking of arrival times and by inaccurate theoretical travel times calculated in the inaccurate velocity model.

The density function of the arrival–time residuals is

$$\sigma_t(\mathbf{t} - \tilde{\boldsymbol{\tau}}^0) = \exp[-\frac{1}{2}(\mathbf{t} - \tilde{\boldsymbol{\tau}}^0)^T \mathbf{S}^{-1}(\mathbf{t} - \tilde{\boldsymbol{\tau}}^0)] \quad , \quad (30)$$

where

$$\tilde{\boldsymbol{\tau}}^0 = \boldsymbol{\tau}^0 + \mathbf{E} x_4^0 \quad . \quad (31)$$

Complete arrival–time covariance matrix \mathbf{S} is given by definition (10). Since $N \times N$ matrix $\mathbf{C}^{-1} - \mathbf{C}^{-1}\mathbf{P}(\mathbf{P}^T\mathbf{C}^{-1}\mathbf{P})^{-1}\mathbf{P}^T\mathbf{C}^{-1}$ has rank $N-4$ with null space generated by the three columns of matrix \mathbf{P} and by vector \mathbf{E} , arrival–time misfit (28) does not depend on the hypocentral time,

$$y = (\mathbf{t} - \tilde{\boldsymbol{\tau}}^0)^T [\mathbf{C}^{-1} - \mathbf{C}^{-1}\mathbf{P}(\mathbf{P}^T\mathbf{C}^{-1}\mathbf{P})^{-1}\mathbf{P}^T\mathbf{C}^{-1}] (\mathbf{t} - \tilde{\boldsymbol{\tau}}^0) \quad . \quad (32)$$

We introduce new arrival–time coordinates

$$\boldsymbol{\xi} = \mathbf{S}^{-\frac{1}{2}}(\mathbf{t} - \tilde{\boldsymbol{\tau}}^0) \quad , \quad (33)$$

and the density function (28) of the arrival–time residuals simplifies to

$$\sigma_\xi(\boldsymbol{\xi}) = \exp(-\frac{1}{2}\boldsymbol{\xi}^T \boldsymbol{\xi}) \quad . \quad (34)$$

Arrival–time misfit (32) then becomes

$$y = \boldsymbol{\xi}^T \mathbf{A} \boldsymbol{\xi} \quad , \quad (35)$$

where

$$\mathbf{A} = \mathbf{S}^{\frac{1}{2}} [\mathbf{C}^{-1} - \mathbf{C}^{-1}\mathbf{P}(\mathbf{P}^T\mathbf{C}^{-1}\mathbf{P})^{-1}\mathbf{P}^T\mathbf{C}^{-1}] \mathbf{S}^{\frac{1}{2}} \quad . \quad (36)$$

The square of matrix \mathbf{A} is

$$\mathbf{A}\mathbf{A} = \mathbf{S}^{\frac{1}{2}} [\mathbf{1} - \mathbf{C}^{-1}\mathbf{P}(\mathbf{P}^T\mathbf{C}^{-1}\mathbf{P})^{-1}\mathbf{P}^T] \mathbf{C}^{-1} \mathbf{S} \mathbf{C}^{-1} [\mathbf{1} - \mathbf{P}(\mathbf{P}^T\mathbf{C}^{-1}\mathbf{P})^{-1}\mathbf{P}^T\mathbf{C}^{-1}] \mathbf{S}^{\frac{1}{2}} \quad . \quad (37)$$

Since

$$\mathbf{C}^{-1} \mathbf{S} \mathbf{C}^{-1} = \mathbf{C}^{-1} \quad , \quad (38)$$

see (19), the square of matrix \mathbf{A} reads

$$\mathbf{A}\mathbf{A} = \mathbf{S}^{\frac{1}{2}} [\mathbf{1} - \mathbf{C}^{-1}\mathbf{P}(\mathbf{P}^T\mathbf{C}^{-1}\mathbf{P})^{-1}\mathbf{P}^T] \mathbf{C}^{-1} [\mathbf{1} - \mathbf{P}(\mathbf{P}^T\mathbf{C}^{-1}\mathbf{P})^{-1}\mathbf{P}^T\mathbf{C}^{-1}] \mathbf{S}^{\frac{1}{2}} \quad , \quad (39)$$

and we see that \mathbf{A} is an $N \times N$ projection matrix,

$$\mathbf{A} \mathbf{A} = \mathbf{A} \quad . \quad (40)$$

Projection matrix \mathbf{A} is an $N \times N$ matrix of rank $N-4$ with null space generated by the three columns of matrix $\mathbf{S}^{-\frac{1}{2}} \mathbf{P}$ and by vector $\mathbf{S}^{-\frac{1}{2}} \mathbf{E}$.

The mean value of any function $y(\boldsymbol{\xi})$ of the arrival-time residuals is

$$\langle y \rangle = \int y(\boldsymbol{\xi}) \sigma_{\xi}(\boldsymbol{\xi}) \, d^N \xi \left[\int \sigma_{\xi}(\boldsymbol{\xi}) \, d^N \xi \right]^{-1} \quad , \quad (41)$$

which reads

$$\langle y \rangle = \int y(\boldsymbol{\xi}) \exp(-\frac{1}{2} \boldsymbol{\xi}^T \boldsymbol{\xi}) \, d^N \xi \left[\int \exp(-\frac{1}{2} \boldsymbol{\xi}^T \boldsymbol{\xi}) \, d^N \xi \right]^{-1} \quad . \quad (42)$$

We select ξ_J , $J = N-3, \dots, N$ in the kernel of \mathbf{A} . Then

$$y(\boldsymbol{\xi}) = \sum_{J=1}^{N-4} (\xi_J)^2 \quad (43)$$

is independent of ξ_J , $J = N-3, \dots, N$. We thus integrate with respect to ξ_J , $J = N-3, \dots, N$ and reduce the fraction.

In the subspace ξ_J , $J = 1, \dots, N-4$, we introduce spherical coordinates with

$$r = \sqrt{\sum_{J=1}^{N-4} (\xi_J)^2} \quad . \quad (44)$$

Then

$$y(\boldsymbol{\xi}) = r^2 \quad , \quad (45)$$

and mean value (42) reads

$$\langle y \rangle = \int r^2 r^{N-5} \exp(-\frac{1}{2} r^2) \, dr \left[\int r^{N-5} \exp(-\frac{1}{2} r^2) \, dr \right]^{-1} \quad . \quad (46)$$

We introduce integration variable $\rho = \frac{1}{2} r^2$,

$$\langle y \rangle = \int 2 \rho^{\frac{N-4}{2}} \exp(-\rho) \, d\rho \left[\int \rho^{\frac{N-6}{2}} \exp(-\rho) \, d\rho \right]^{-1} \quad , \quad (47)$$

and calculate the integrals. The mean value of the arrival-time misfit is

$$\langle y \rangle = N-4 \quad . \quad (48)$$

We can analogously calculate

$$\langle y^2 \rangle = \int r^4 r^{N-5} \exp(-\frac{1}{2} r^2) \, dr \left[\int r^{N-5} \exp(-\frac{1}{2} r^2) \, dr \right]^{-1} \quad , \quad (49)$$

which reads

$$\langle y^2 \rangle = \int 4 \rho^{\frac{N-2}{2}} \exp(-\rho) \, d\rho \left[\int \rho^{\frac{N-6}{2}} \exp(-\rho) \, d\rho \right]^{-1} = (N-2)(N-4) \quad , \quad (50)$$

and calculate the integrals. The standard deviation of the arrival-time misfit is then

$$\sqrt{\langle (y - \langle y \rangle)^2 \rangle} = \sqrt{\langle y^2 \rangle - \langle y \rangle^2} = \sqrt{2(N-4)} \quad . \quad (51)$$

5. Model covariance function

The proposed nonlinear hypocentre determination yields nonnormalized marginal a posteriori density function (18), which describes the relative probability of the seismic hypocentre. In addition, the proposed nonlinear hypocentre determination also yields arrival-time misfit (29). This arrival-time misfit can be used to check the model covariance function used to calculate matrix Θ of geometrical covariances of theoretical travel times, appearing in theoretical density function (2).

The mean value of the arrival-time misfit should correspond to estimation (48). We thus calculate the average \bar{y} of arrival-time misfit (29) for many determined hypocentres, and the average $\overline{N-4}$ of the right-hand sides of estimation (48).

If \bar{y} is significantly greater than $\overline{N-4}$, the model covariance function is underestimated, i.e., the velocity model is less accurate than suggested by the model covariance function.

If \bar{y} is significantly smaller than $\overline{N-4}$, the model covariance function is overestimated, i.e., the velocity model is more accurate than suggested by the model covariance function.

As a rule, we are using both P-wave and S-wave velocity models in isotropic media. If the number of recorded arrivals is sufficient, we may apply the proposed nonlinear hypocentre determination to P-wave arrivals only, and check the model covariance function of the P-wave velocity model using the above described procedure. Analogously, we may apply the proposed nonlinear hypocentre determination to S-wave arrivals only, and check the model covariance function of the S-wave velocity model using the above described procedure. Finally, we may apply the proposed nonlinear hypocentre determination to all arrivals, and check the model covariance functions of both the P-wave and S-wave velocity models simultaneously.

6. Inaccurate simplified numerical implementation of the algorithm

For the hypocentre determination, we need mean values \mathbf{t} of the measured arrival times at the receivers, and data covariance matrix \mathbf{T} describing their inaccuracy. The data covariance matrix is usually diagonal, composed of the squares of the standard deviations of the measured arrival times. Note that a receiver recording both P and S waves is formally doubled into the P-wave receiver and the S-wave receiver. Analogously for other waves like reflected or converted.

Theoretical travel times $\tau(x_i)$ from the nodes x_i of a spatial grid of points to the receivers can simply be calculated by interpolation within ray cells (Bulant, 1996; 1997; 1999; Bulant & Klimeš, 1999; Bulant, 2012). For each receiver, we obtain a spatial grid of discretized travel times.

The calculation and storage of the matrix Θ of geometrical covariances of theoretical travel times (Klimeš, 2008) is more difficult, because we have a spatial grid of the discretized element of matrix Θ for each couple of receivers.

6.1. Approximation of geometrical covariances of theoretical travel times

For the sake of simplicity, we assume the model covariance function of the slowness in the form

$$C(x_m^1, x_n^2) = \rho^2 u(x_m^1) u(x_n^2) \left(\frac{(x_i^1 - x_i^2)(x_i^1 - x_i^2)}{\theta^2} \right)^H \left(\frac{u(x_k^1) + u(x_k^2)}{2} \right)^{2H}, \quad (52)$$

where $u(x_i)$ is the slowness at point x_i and constant θ is the reference travel time. Model covariance function (52) is determined by the Hurst exponent H and by the relative slowness variation ρ at the distance corresponding to the reference travel time.

The diagonal elements of the matrix Θ of geometrical covariances of theoretical travel times then approximately read (Klimeš, 2002c, eq. 30)

$$\Theta_{KK} = \frac{2\rho^2\theta^2}{(2H+1)(2H+2)} \left(\frac{\tau_K}{\theta} \right)^{2+2H}. \quad (53)$$

We introduce the standard deviation

$$\sigma = \rho\theta \sqrt{\frac{2}{(2H+1)(2H+2)}} \quad (54)$$

of theoretical travel times corresponding to reference travel time θ . Diagonal elements (53) then read

$$\Theta_{KK} = \sigma^2 \left(\frac{\tau_K}{\theta} \right)^{2+2H}. \quad (55)$$

These geometrical variances of theoretical travel times are simple functions of travel times discretized at the nodes of a spatial grid of points used for the hypocentre determination.

On the other hand, the calculation and storage of the off-diagonal elements of matrix Θ of geometrical covariances of theoretical travel times is difficult. In order to speed up the development of a numerical algorithm and to start with the numerical tests, we put all off-diagonal elements of matrix Θ equal to zeros, which is obviously incorrect. We thus perform the hypocentre determination described in previous sections with incorrect matrix (10) and consequently with incorrect matrix (19).

6.2. Numerical algorithm of nonlinear hypocentre determination

Hypocentral time (14), its standard deviation (16) and the nonnormalized 3-D marginal a posteriori density function (17) are composed of quantities $a = \mathbf{E}^T \mathbf{S}^{-1} \mathbf{E}$, $b = \mathbf{E}^T \mathbf{S}^{-1} (\mathbf{t} - \boldsymbol{\tau})$ and $d = (\mathbf{t} - \boldsymbol{\tau})^T \mathbf{S}^{-1} (\mathbf{t} - \boldsymbol{\tau})$ or $c = d - b^2/a$, which can be accumulated gradually for individual arrival times. The corresponding numerical algorithm has been proposed by Bucha & Klimeš (2015, sec. 2.2) under the assumption of the diagonal matrix of geometrical covariances of theoretical travel times.

6.3. Error of the inaccurate numerical algorithm

In Section 4, we assumed that matrix \mathbf{S} given by definition (10) is correct. If matrix \mathbf{S} is incorrect, Section 4 is no longer applicable.

In such a case, the density function (30) of the arrival-time residuals reads

$$\sigma_t(\mathbf{t} - \tilde{\boldsymbol{\tau}}^0) = \exp[-\frac{1}{2}(\mathbf{t} - \tilde{\boldsymbol{\tau}}^0)^T \tilde{\mathbf{S}}^{-1}(\mathbf{t} - \tilde{\boldsymbol{\tau}}^0)] \quad , \quad (56)$$

where $\tilde{\mathbf{S}}$ is the correct matrix (10), whereas matrix \mathbf{C} in arrival-time misfit (32) is calculated using the incorrect matrix \mathbf{S} .

The mean value of the function (32) of \mathbf{t} then reads

$$\langle y \rangle = \text{tr}\{\tilde{\mathbf{S}}[\mathbf{C}^{-1} - \mathbf{C}^{-1}\mathbf{P}(\mathbf{P}^T\mathbf{C}^{-1}\mathbf{P})^{-1}\mathbf{P}^T\mathbf{C}^{-1}]\} \quad , \quad (57)$$

which can be expressed in terms of matrix (36) as

$$\langle y \rangle = \text{tr}(\tilde{\mathbf{S}}\mathbf{S}^{-\frac{1}{2}}\mathbf{A}\mathbf{S}^{-\frac{1}{2}}) \quad . \quad (58)$$

We define $N \times 4$ matrix $\tilde{\mathbf{P}}$ composed of the three columns of matrix \mathbf{P} and of vector \mathbf{E} . Since matrix (36) is a projection matrix of rank $N-4$ with null space generated by the columns of matrix $\mathbf{S}^{-\frac{1}{2}}\tilde{\mathbf{P}}$, we may express it in form

$$\mathbf{A} = \mathbf{1} - \mathbf{S}^{-\frac{1}{2}}\tilde{\mathbf{P}}(\tilde{\mathbf{P}}^T\mathbf{S}^{-1}\tilde{\mathbf{P}})^{-1}\tilde{\mathbf{P}}^T\mathbf{S}^{-\frac{1}{2}} \quad . \quad (59)$$

Mean arrival-time misfit (58) resulting from the inaccurate numerical algorithm can then be expressed as

$$\langle y \rangle = N - 4 - \text{tr}[(\tilde{\mathbf{S}} - \mathbf{S})\mathbf{S}^{-1}\tilde{\mathbf{P}}(\tilde{\mathbf{P}}^T\mathbf{S}^{-1}\tilde{\mathbf{P}})^{-1}\tilde{\mathbf{P}}^T\mathbf{S}^{-1}] \quad . \quad (60)$$

Here matrix $\tilde{\mathbf{S}} - \mathbf{S}$ is composed of all neglected off-diagonal elements of matrix $\boldsymbol{\Theta}$. All these elements are positive. Mean arrival-time misfit $\langle y \rangle$ resulting from the inaccurate numerical algorithm is thus considerably smaller than the correct arrival-time misfit (48).

Due to the inaccurate numerical algorithm, the velocity model seems to be more accurate than it actually is, and the model covariance function seems overestimated even if it were underestimated.

7. Numerical example

We use the numerical algorithm proposed by Bucha & Klimeš (2015, sec. 2.2) under the assumption of the diagonal matrix of geometrical covariances of theoretical travel times. The algorithm of nonlinear hypocentre determination consists in calculations at the nodes of a 3-D grid of points, and has been coded in the form of command files `loc0.cal`, `loc1.cal` and `loc2.cal` for program `grdcal.for` which performs calculations at the nodes of a grid of points. Command files `loc0.cal`, `loc1.cal` and `loc2.cal` are located in package FORMS (Bucha, Bulant & Klimeš, 2000). For the nonlinear hypocentre determination, we use software packages FORMS, MODEL and CRT (Bucha & Bulant, 2015).

We test the hypocentre determination algorithm on the data from microseismic monitoring of natural microearthquakes appearing during a period of one year in an unknown locality. The monitoring array consisted of 15 surface receivers irregularly distributed in the area. Not all receivers worked continuously, none of the events was strong enough to be registered at all receivers.

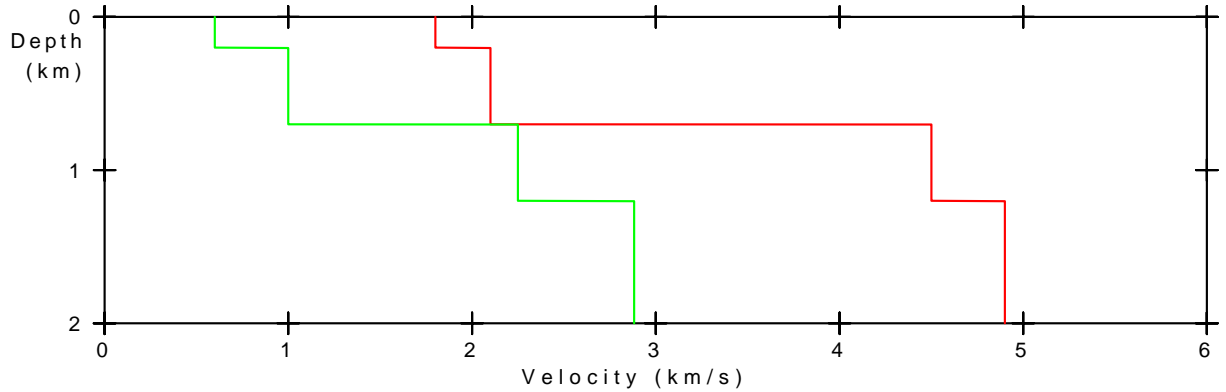


Figure 1: The P–wave velocity (red) and S–wave velocity (green) in the laterally homogeneous one–dimensional velocity model.

The velocity model available for the locality is one–dimensional, and is displayed in Figure 1. It consists of three homogeneous layers and a homogeneous halfspace. The depths of the layer boundaries are 200 m, 700 m and 1200 m, the values of P–wave velocity in the layers are 1800 m/s, 2100 m/s, 4500 m/s and 4900 m/s (from the top to the bottom), the values of S–wave velocity are 600 m/s, 1000 m/s, 2250 m/s and 2882 m/s.

Unfortunately, we do not know the P–wave and S–wave model covariance functions describing the uncertainty of the velocity model.

In order to try to determine the hypocentres in this unfortunate situation, we have to fabricate very rough estimates of the P–wave and S–wave model covariance functions. We assume the power–law covariance functions (52) of a self–affine random medium (Klimeš, 2002b; 2002c). Since we have no possibility to determine the Hurst exponent, we use the value

$$H = -0.12 \quad (61)$$

determined by Klimeš (2002c) as acceptable for the Western Bohemia region, although we know that our locality is placed in a different part of the world. We use

$$\theta = 1 \text{ s} \quad (62)$$

as the reference travel time in the variances (55) of the theoretical travel times.

We then attempt to determine factors σ_P and σ_S in variances (55) for P waves and S waves using the mean arrival–time misfits resulting from the hypocentre determination, although we know from Section 6.2 that we shall obtain smaller values of σ_P and σ_S than the actual ones, because we neglect all off–diagonal elements of matrix Θ of the geometrical covariances of theoretical travel times.

We use the location grid of dimensions 48.300 km \times 49.950 km \times 9.000 km, composed of 323 \times 334 \times 31 gridpoints with grid intervals 0.150 km \times 0.150 km \times 0.300 km. The top of the location grid is situated at the depth of 0.800 km.

We have the arrival time of 33 seismic events. For the determination of the P–wave and S–wave model covariance functions, we selected 30 events for which at least six P–wave arrival times and at least six S–wave arrival times have been measured, see Table 1. The assumed standard deviations of picking is 0.004 s for all arrival times.

We determined the nonnormalized 3–D marginal a posteriori density function (55) just from the P–wave arrival times for the 30 selected events using various values of factor σ_P in variances (55). We then chose the value of

$$\sigma_P = 0.039 \text{ s} \quad (63)$$

Event	N_P	N_S	y_P	y_S	y_{P+S}
01	8	7	2.693	1.471	6.656
02	9	7	4.631	2.776	11.189
03	8	7	3.172	1.823	7.673
04	8	7	3.527	2.082	8.486
05	8	6	2.452	1.590	5.636
06	8	7	2.955	1.662	7.038
07	8	7	3.767	2.167	9.060
08	8	7	3.186	1.809	7.601
09	9	7	4.360	1.580	9.181
10	5	5			
11	8	7	3.000	2.969	8.833
12	4	4			
13	8	7	7.124	3.752	21.344
14	9	8	6.625	4.533	25.573
15	9	9	5.674	8.439	16.794
16	9	9	5.062	6.335	13.235
17	9	7	10.407	1.342	17.272
18	9	9	4.211	5.522	12.666
19	9	8	3.830	3.445	8.691
20	9	8	2.756	2.846	6.656
21	9	7	3.893	1.741	6.970
22	9	8	3.154	2.140	6.200
23	9	9	3.869	3.084	8.964
24	9	8	6.564	6.355	15.421
25	9	9	10.732	12.631	25.050
26	8	8	5.837	8.220	18.836
27	9	9	5.518	8.105	14.547
28	9	8	3.916	1.932	7.890
29	5	3			
30	8	8	3.675	4.818	12.946
31	8	7	3.591	3.988	11.129
32	8	6	5.314	1.011	7.535
33	7	7	1.869	3.084	7.751
Average	8.5	7.6	4.579	3.775	11.561

Table 1: Arrival-time misfits (29) for the 30 selected hypocentres. The first column contains just the names of the events, N_P is the number of measured P-wave arrival times, N_S is the number of measured S-wave arrival times, y_P is arrival-time misfit (29) determined just from the P-wave arrival times, y_S is arrival-time misfit (29) determined just from the S-wave arrival times, y_{P+S} is arrival-time misfit (29) determined from both the P-wave and S-wave arrival times. We have excluded events 10, 12 and 29 when determining factors σ_P and σ_S of the P-wave and S-wave geometrical travel-time variances (55).

for which we obtained a good agreement between the average

$$\overline{y_P} = 4.579 \quad (64)$$

of arrival–time misfit (29) for the 30 selected hypocentres determined from the P–wave arrivals, and the average

$$\overline{N_P} - 4 = 4.500 \quad (65)$$

of the right–hand sides of estimation (48). The agreement is considered with respect to the standard deviation of $\overline{y_P}$, which is

$$\sqrt{\langle (y_P - \langle y_P \rangle)^2 \rangle / 30} = \sqrt{2(\overline{N_P} - 4) / 30} = 0.548 \quad , \quad (66)$$

see (51). We then determined the nonnormalized 3–D marginal a posteriori density function (55) just from the S–wave arrival times for the 30 selected events using various values of factor σ_S in variances (55). We chose the value of

$$\sigma_S = 0.035 \text{ s} \quad (67)$$

for which we obtained a good agreement between the average

$$\overline{y_S} = 3.775 \quad (68)$$

of arrival–time misfit (29) for the 30 selected hypocentres determined from the S–wave arrivals, and the average

$$\overline{N_S} - 4 = 3.600 \quad (69)$$

of the right–hand sides of estimation (48). The agreement is considered with respect to the standard deviation of $\overline{y_S}$, which is

$$\sqrt{\langle (y_S - \langle y_S \rangle)^2 \rangle / 30} = \sqrt{2(\overline{N_S} - 4) / 30} = 0.490 \quad , \quad (70)$$

see (51). We finally determined the nonnormalized 3–D marginal a posteriori density function (55) from both the P–wave arrival times and S–wave arrival times for the 30 selected events using factors (63) and (67). We then can compare the average

$$\overline{y_{P+S}} = 11.561 \quad (71)$$

of arrival–time misfit (29) for the 30 selected hypocentres, determined from both the P–wave and S–wave arrivals, with the average

$$\overline{N_P} + \overline{N_S} - 4 = 12.100 \quad (72)$$

of the right–hand sides of estimation (48). Considering the standard deviation of $\overline{y_{P+S}}$, which is

$$\sqrt{\langle (y_{P+S} - \langle y_{P+S} \rangle)^2 \rangle / 30} = \sqrt{2(\overline{N_P} + \overline{N_S} - 4) / 30} = 0.898 \quad , \quad (73)$$

we see that the above average values are in a good agreement.

Although we used the incorrect P–wave and S–wave geometrical travel–time covariance matrices Θ_P and Θ_S restricted just to the diagonal elements, the behaviour of the nonlinear hypocentre determination is reasonable to the effect that the average arrival–time misfit determined from both the P–wave and S–wave arrivals behaves in the same way it should behave for the correct geometrical travel–time covariance matrices.

Using geometrical travel–time covariance matrices (55) with factors (63) and (67) determined from the 30 selected events, we calculated nonnormalized 3–D marginal

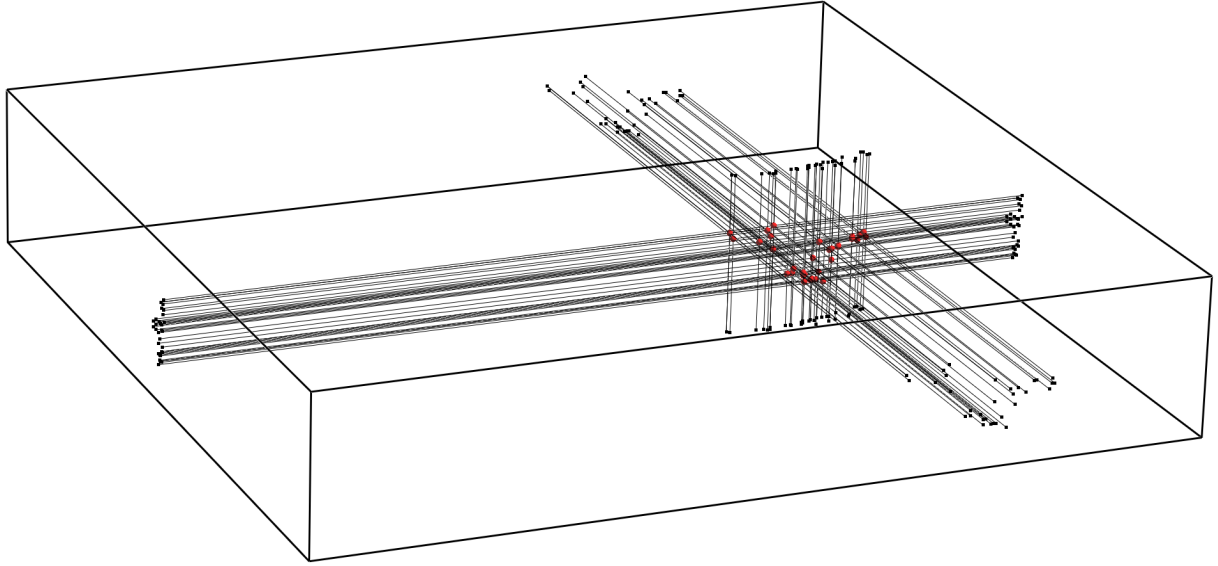


Figure 2: The locations of the maximum values of the 33 nonnormalized 3-D marginal a posteriori density functions describing the relative probability of the seismic hypocentres corresponding to the 33 considered events (small red spheres), together with their projections onto the sides of the grid used for the nonlinear hypocentre determination. The nonnormalized 3-D marginal a posteriori density functions have been determined using both the P-wave and S-wave arrivals. The displayed dimensions of the grid used for the nonlinear hypocentre determination are $48.300 \text{ km} \times 49.950 \text{ km} \times 9.000 \text{ km}$.

a posteriori density functions (18) of the hypocentres of all 33 events using just the P-wave arrival times, using just the S-wave arrival times, and using both the P-wave and S-wave arrival times.

When we inspected the nonnormalized 3-D marginal a posteriori density functions (18) determined using just the P-wave arrival times or using just the S-wave arrival times, we realized that the depth of the hypocenters is uncertain for approximately 75% of events in these cases. This ratio is independent of the number of measured P-wave arrival times or S-wave arrival times in the sense that the hypocentral depth is uncertain in these cases for approximately 75% of events even for 9 measured P-wave arrival times or 9 measured S-wave arrival times.

The locations of the maximum values of 33 nonnormalized 3-D marginal a posteriori density functions (18) describing the relative probability of the seismic hypocentres, determined using both the P-wave and S-wave arrivals, are displayed in Figure 2.

Six examples of the nonnormalized marginal a posteriori density functions (18) describing the relative probability of the seismic hypocentres, determined using both the P-wave and S-wave arrivals, are displayed in Figures 3 and 4. The details of these nonnormalized marginal a posteriori density functions are displayed in Figures 5 and 6. We can observe that the uncertainty of the hypocentral position increases with increasing depth and decreasing number of measured arrival times.

8. Conclusions

In this paper, we considered the robust nonlinear approach to hypocentre determination proposed by Tarantola & Valette (1982), consisting in direct evaluation of the nonnormalized 3-D marginal a posteriori density function which describes the relative probability of the seismic hypocentre, and together with Bucha & Klimeš (2015) proposed the corresponding numerical algorithm. The nonnormalized 3-D marginal a posteriori density function is discretized at the gridpoints of a sufficiently dense 3-D spatial grid of points and yields complete information on the uncertainty of the hypocentre position.

The maximum value of the nonnormalized 3-D marginal a posteriori density function allows for testing the model covariance function describing the uncertainty of the velocity model, and for testing the consistency of measured arrival times. If the number of measured arrival times corresponding to a reasonably numerous subset of events is sufficiently large, we can also very roughly estimate the P-wave and S-wave model covariance functions describing the uncertainty of the velocity model. The P-wave and S-wave model covariance functions are projected onto the uncertainty of the hypocentral position through the geometrical covariances of theoretical travel times calculated in the velocity model. In a case of an error in measured arrival times, we may be able to identify the erroneous data.

For the sake of simplicity and rapid numerical implementation, we considered just the diagonal elements of the geometrical travel-time covariance matrix in this paper. This incorrect simplification leads to the distortion of the nonnormalized 3-D marginal a posteriori density function, and especially to the incorrect increment of its maximum value. If the number of measured arrival times corresponding to a reasonably numerous subset of events is sufficiently large, we can reduce this distortion of the nonnormalized 3-D marginal a posteriori density function by artificially decreasing the multiplicative factors of the P-wave and S-wave model covariance functions.

In the numerical example, we estimated the multiplicative factors of the P-wave model covariance function using just the P-wave arrivals, and the multiplicative factors of the S-wave model covariance function using just the S-wave arrivals. Although we used the incorrect P-wave and S-wave geometrical travel-time covariance matrices restricted just to the diagonal elements, the behaviour of the nonlinear hypocentre determination in the numerical example was reasonable to the effect that the average arrival-time misfit determined using both the P-wave and S-wave arrivals behaved in the same way it should behave for the correct geometrical travel-time covariance matrices.

We are going to propose the numerical algorithm of calculating the whole geometrical travel-time covariance matrix at the gridpoints of a 3-D spatial grid in the near future.

Acknowledgements

The research has been supported by the Grant Agency of the Czech Republic under contract P210/10/0736, by the Ministry of Education of the Czech Republic within research projects MSM0021620860 and CzechGeo/EPOS LM2010008, and by the members of the consortium “Seismic Waves in Complex 3-D Structures” (see “<http://sw3d.cz>”).

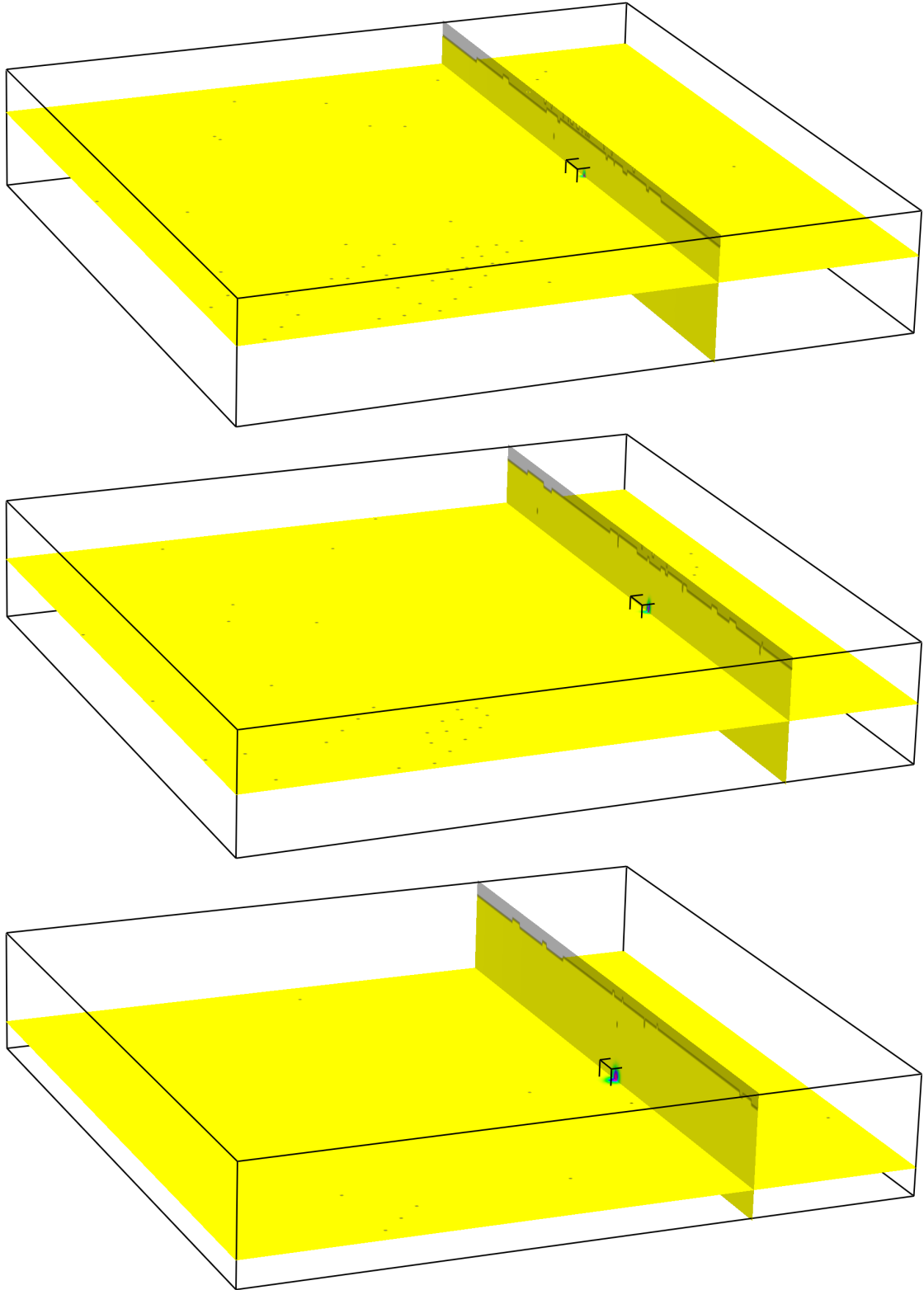


Figure 3: Nonnormalized 3-D marginal a posteriori density functions (18) determined using both the P-wave and S-wave arrivals with maxima located in different depths. The zero values are displayed in yellow. The nonzero values range through green, cyan, blue and magenta to the maximum value displayed in red. The undefined values are displayed in gray, and denote the gridpoints at which at least one theoretical travel time is missing. The small cubes centred at the maxima have the sides of 2 km. **Top:** event 23 (9+9 arrival times), **middle:** event 25 (9+9 arrival times), **bottom:** event 09 (9+7 arrival times).

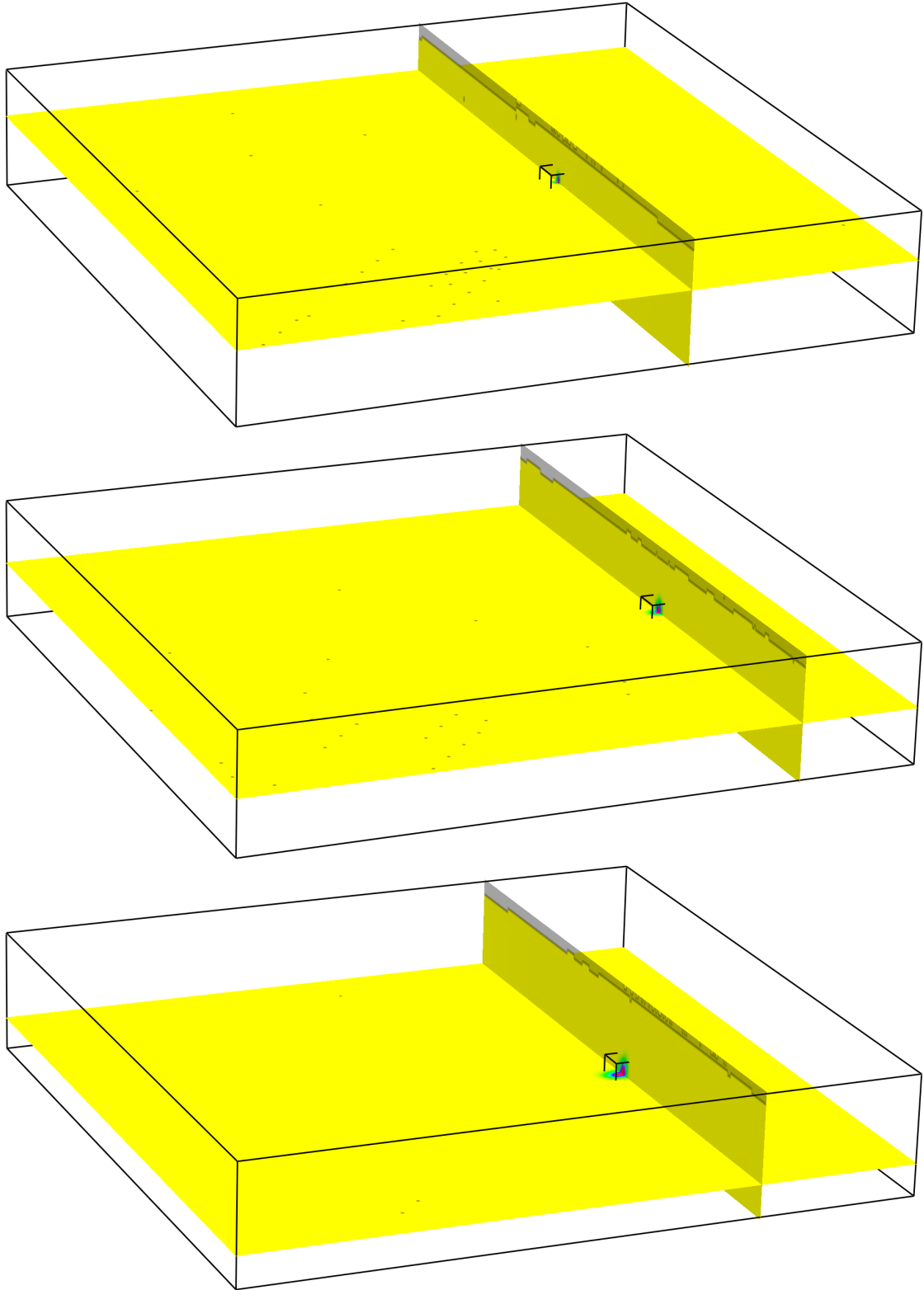


Figure 4: Nonnormalized 3-D marginal a posteriori density functions (18) determined using both the P-wave and S-wave arrivals for the events located in similar depths as in Figure 3, but with smaller numbers of measured P-wave and S-wave arrivals. The zero values are displayed in yellow. The nonzero values range through green, cyan, blue and magenta to the maximum value displayed in red. The undefined values are displayed in gray, and denote the gridpoints at which at least one theoretical travel time is missing. The small cubes centred at the maxima have the sides of 2 km. **Top:** event 32 (8+6 arrival times), **middle:** event 13 (8+7 arrival times), **bottom:** event 12 (4+4 arrival times).

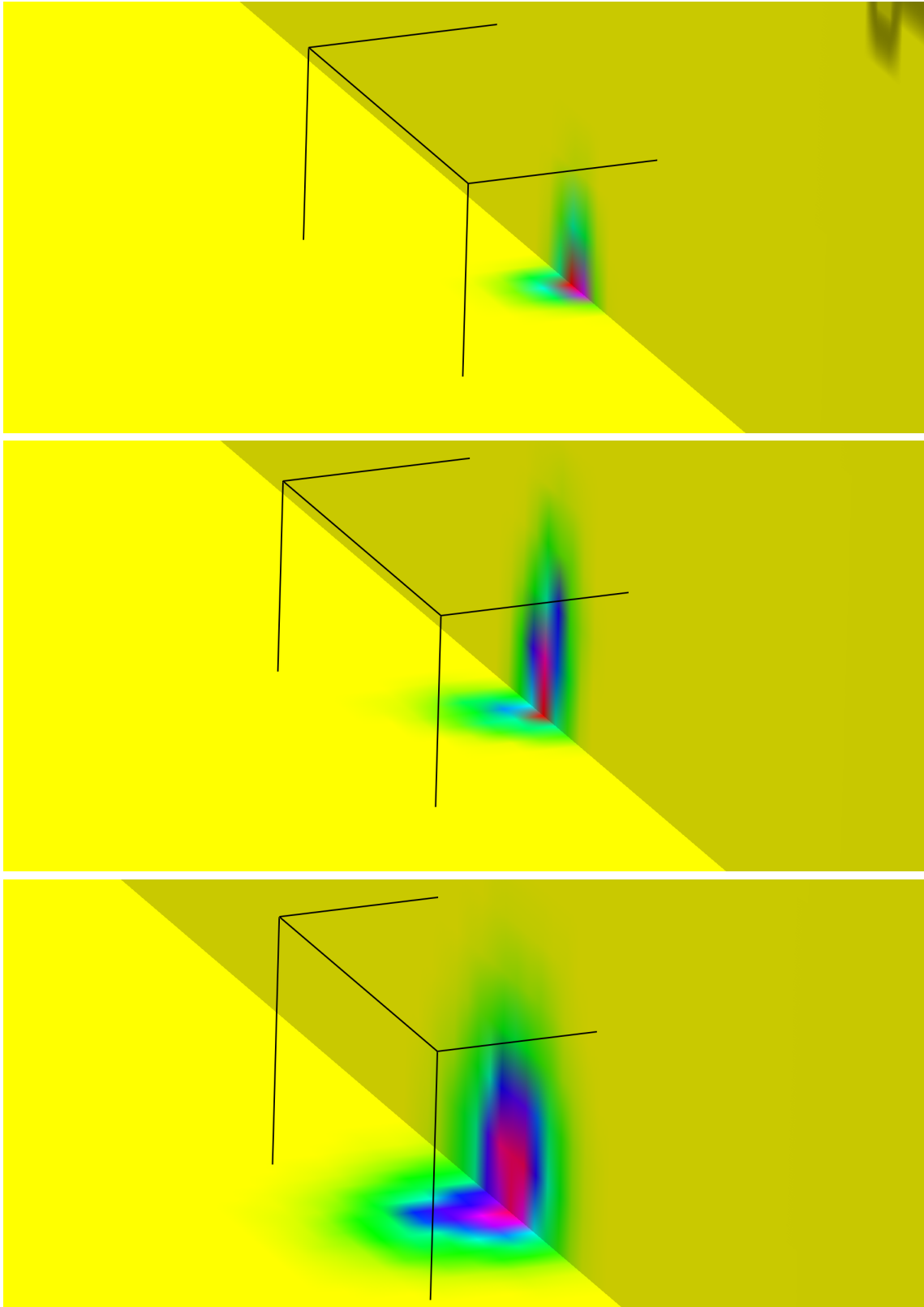


Figure 5: The details of the interpolated discretized nonnormalized 3-D marginal a posteriori density functions (18) of Figure 3 displaying the hypocentral regions. The cubes centred at the maxima have the sides of 2 km. **Top:** event 23 (9+9 arrival times), **middle:** event 25 (9+9 arrival times), **bottom:** event 09 (9+7 arrival times).

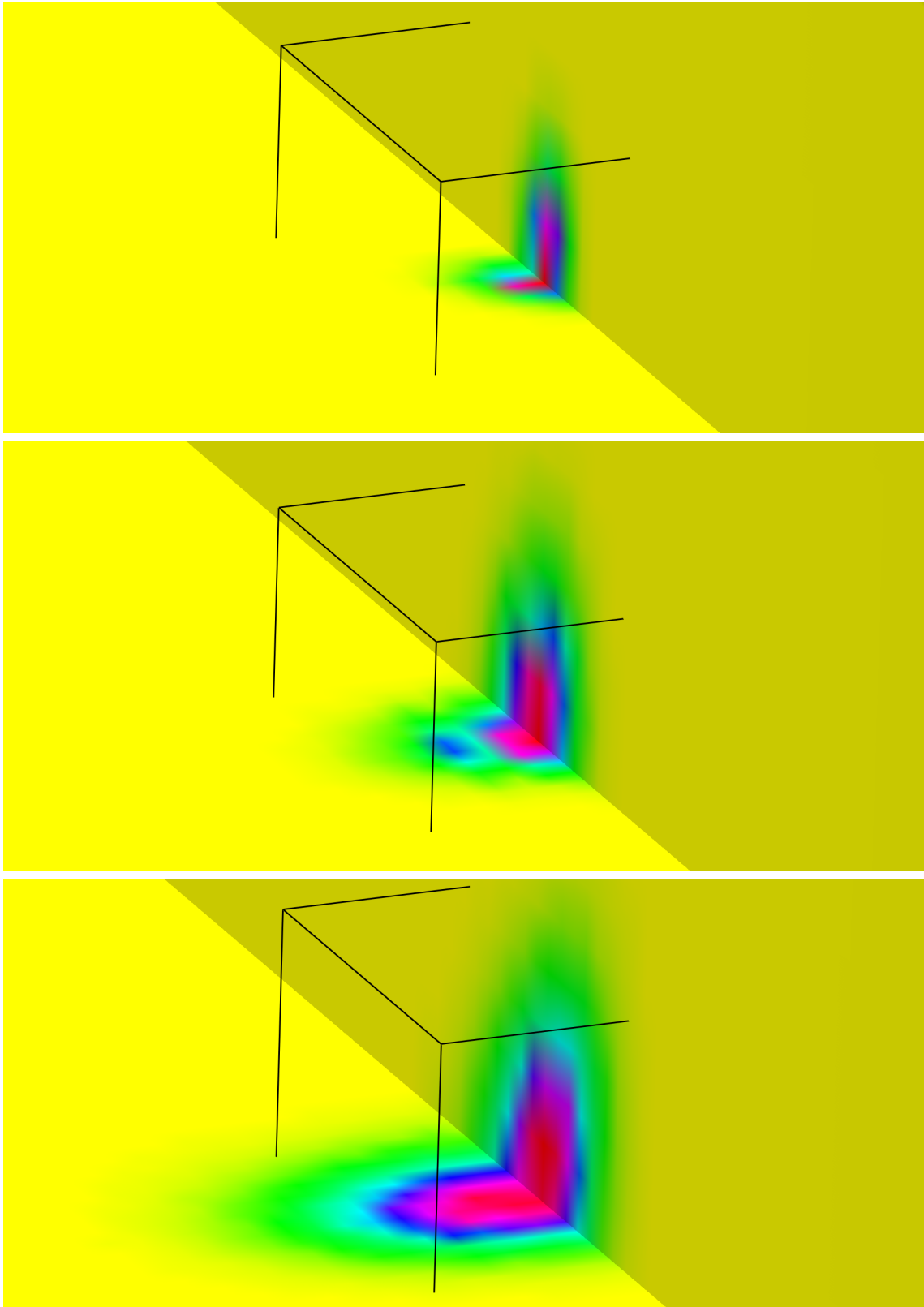


Figure 6: The details of the interpolated discretized nonnormalized 3-D marginal a posteriori density functions (18) of Figure 4 displaying the hypocentral regions. Compared to Figure 5, we can observe larger hypocentre uncertainty due to smaller number of measured arrival times. The cubes centred at the maxima have the sides of 2 km. **Top:** event 32 (8+6 arrival times), **middle:** event 13 (8+7 arrival times), **bottom:** event 12 (4+4 arrival times).

References

- Bucha, V. & Bulant, P. (eds.) (2015): SW3D-CD-19 (DVD-ROM). *Seismic Waves in Complex 3-D Structures*, **25**, 209–210, online at “<http://sw3d.cz>”.
- Bucha, V., Bulant, P. & Klimeš, L. (eds.) (2000): SW3D-CD-4 (CD-ROM). *Seismic Waves in Complex 3-D Structures*, **10**, 227–227, online at “<http://sw3d.cz>”.
- Bucha, V. & Klimeš, L. (2015): Nonlinear hypocentre determination in the 3-D Western Bohemia a priori velocity model. *Seismic Waves in Complex 3-D Structures*, **25**, 37–50, online at “<http://sw3d.cz>”.
- Bulant, P. (1996): Two-point ray tracing in 3-D. *Pure appl. Geophys.*, **148**, 421–447.
- Bulant, P. (1997): Calculation of multivalued ray-theory travel times at nodes of 3-D grids. *Seismic Waves in Complex 3-D Structures*, **6**, 71–74, online at “<http://sw3d.cz>”.
- Bulant, P. (1999): Two-point ray-tracing and controlled initial-value ray-tracing in 3-D heterogeneous block structures. *J. seism. Explor.*, **8**, 57–75, online at “<http://sw3d.cz>”.
- Bulant, P. (2012): Interpolation within ray tubes — state of the art. *Seismic Waves in Complex 3-D Structures*, **22**, 169–182, online at “<http://sw3d.cz>”.
- Bulant, P. & Klimeš, L. (1999): Interpolation of ray theory traveltimes within ray cells. *Geophys. J. int.*, **139**, 273–282, online at “<http://sw3d.cz>”.
- Franklin, J.N. (1970): Well-posed stochastic extensions of ill-posed linear problems. *J. math. Anal. Appl.*, **31**, 682–716.
- Klimeš, L. (1996): Arrival-time residuals and hypocentre mislocation. *Pure appl. Geophys.*, **148**, 337–342, online at “<http://sw3d.cz>”.
- Klimeš, L. (2002a): Application of the medium covariance functions to travel-time tomography. *Pure appl. Geophys.*, **159**, 1791–1810, online at “<http://sw3d.cz>”.
- Klimeš, L. (2002b): Correlation functions of random media. *Pure appl. Geophys.*, **159**, 1811–1831, online at “<http://sw3d.cz>”.
- Klimeš, L. (2002c): Estimating the correlation function of a self-affine random medium. *Pure appl. Geophys.*, **159**, 1833–1853, online at “<http://sw3d.cz>”.
- Klimeš, L. (2008): Calculation of the a priori geometrical covariances of travel times in a self-affine random medium. *Seismic Waves in Complex 3-D Structures*, **18**, 27–70, online at “<http://sw3d.cz>”.
- Tarantola, A. (1987): *Inverse Problem Theory*. Elsevier, Amsterdam.
- Tarantola, A. & Nercessian, A. (1984): Three-dimensional inversion without blocks. *Geophys. J. Roy. astr. Soc.*, **76**, 299–306.
- Tarantola, A. & Valette, B. (1982): Inverse problems = quest for information. *J. Geophys.*, **50**, 159–170.